

## Soft sediment deformation structures in late Quaternary abandoned channel fill deposit of Yamuna river in NW Sub-Himalaya, India

Anand K. Pandey\* and Prabha Pandey

CSIR-National Geophysical Research Institute, Uppal Road, Hyderabad 500 007, India

Soft sediment deformation (SSD) structures are observed in a 26–25 ka old fluvio-lacustrine channel-fill deposit in tectonically active Dun valley in NW Sub-Himalaya. This fluvio-lacustrine channel-fill deposit experienced intermittent inundation during initial phase of erosional avulsion with the growth of a plug bar causing complete channel abandonment. The facies depict variation from an active channel to rhythmite and lacustrine deposition in an abandoned channel setting. In the studied section, three zones of SSD structures comprising load structures, contorted beds, slumps, folds and faults are observed. These zones are invariably overlain by undeformed beds suggesting recurrent deformation. The varying geometry of SSD structures suggest gravity-driven viscous–brittle deformation in the sediment column possibly due to differential liquidization in the beds with varying grain size, when the equilibrium was disturbed by a trigger mechanism. Since the region lies in the seismically active Himalayan belt, earthquake-induced strong ground motion may be the most plausible trigger mechanism for the observed SSD in the abandoned channel deposits and slope, sediment overloading or groundwater change may not have played a major role.

**Keywords:** Abandoned channel, rhythmite, soft sediment deformation, Sub-Himalaya, trigger mechanism.

SOFT sediment deformation (SSD) structures is a collective term used to describe various structures developed in unconsolidated sediments, either by *in situ* deformation through relative grain displacements or bulk transport of sediment column, prior to or soon after burial at the sediment–water interface<sup>1</sup>. SSD is mostly driven by liquidization (fluidization and liquefaction) in the sediment column caused by enhanced pore water pressure in response to a triggering mechanism<sup>1,2</sup>. The liquidization in sediment column of varied depositional settings may be caused by surface waves, rapid sedimentation, overloading, slope instability, sudden changes in groundwater level, artesian conditions, escape of pore water/gas as well as seismicity<sup>3–7</sup>; though the list is not exhaustive. Poor preservation and modification of deposits and landforms in geological record often limit the reconstruction

of the depositional setting and the trigger mechanism for the observed SSD<sup>3,4</sup>. The problem is frequent in late Quaternary records of tectonically active regions such as Himalaya, since the region also experienced climate fluctuation during the period that affected the gradational process. In one such late Quaternary fluvio-lacustrine terrace deposit of river Yamuna in northwest (NW) Sub-Himalaya (Figure 1), we observed several zones of SSD structures. We attempt to reconstruct late Quaternary landforms and fluvio-lacustrine depositional setting along Yamuna river in Dun valley and understand the potential trigger mechanism for the observed SSD structures in the sediment column. As the region is also undergoing fast exhumation, corresponding valley floor incision and river bank erosion in response to the late Quaternary climatic–tectonic interaction<sup>8</sup>, we discuss the limitations in the reconstruction of landforms and trigger mechanism for the observed SSD structures, as well.

The study area lies in the confined flood plains of Yamuna river, which flows as a braided channel in Sub-Himalayan Dehra Dun valley (Figure 1a). In Dun valley, the Siwalik Group constitutes the substrate over which the piedmont gravel, fluvial strath and fill terrace were deposited during late Quaternary–Holocene period<sup>9–11</sup>. Six levels of paired and unpaired strath and fill terraces

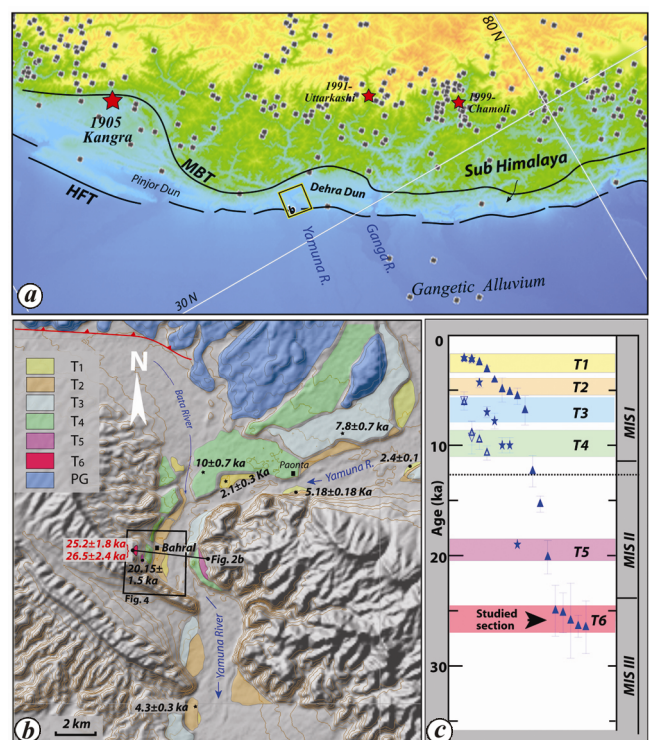


**Figure 1.** a, Various Duns in NW Sub-Himalaya overlaid with the study area along the river Yamuna in Dehra Dun. Note the seismicity in Himalaya since 1976 (data source: USGS Earthquake Catalogue). b, The distribution of late Quaternary–Holocene fluvial terraces along the Yamuna river. c, The OSL ages showing a gradational phases. (MBT, Main Boundary Thrust; HFT, Himalayan Frontal Thrust.)

\*For correspondence. (e-mail: akpandey@ngri.res.in)

(Figure 1b) are mapped along the Yamuna river in Dun valley. The younger four terraces  $T_1$ ,  $T_2$ ,  $T_3$  and  $T_4$  developed during Holocene have widespread distribution, but the older  $T_5$  and  $T_6$  terraces are mapped only at a few locations (Figure 1b). At the studied section near Bahral village,  $T_5$  and  $T_6$  terraces are observed at 40 m and 50–65 m above present stream level with optically stimulated luminescence (OSL) ages of  $20.15 \pm 1.5$  ka and  $26.5 \pm 2.4$  to  $25.2 \pm 1.8$  ka respectively<sup>11</sup> (Figure 1b and c). The  $T_5$  and  $T_4$  terraces have paired surface across the river (Figures 1b and 2) with the unpaired younger terraces showing decreasing relative relief and narrowing of the flood plain from ~5 km to <2 km at present. This suggests a continuous incision of the valley floor at the rate of  $1.96 \pm 0.18$  mm/yr and  $1.98 \pm 0.15$  mm/yr since formation of  $T_6$  and  $T_5$  terraces respectively. Similar incision rate was observed in Holocene terraces of Yamuna river<sup>10</sup>.

A 40–50 m wide and >15 m high scarp section was excavated and logged (Figure 2) in the oldest  $T_6$  terrace deposit to study the SSD structures. In the excavated section, beds are gently dipping towards the centre in the lower part and are horizontal in the upper part with three zones of litho-facies association. The basal zone consists of imbricate, clast-supported stratified gravel (*Gm*) composed of subrounded, moderately well-sorted pebble size clasts with occasional granules and coarse sand lenses. The gravels are overlain by coarse to medium-grained sand and fine granules (*St*) with well-developed cross-stratification, which are >30 cm thick in the middle part of the section and become smaller towards margins (Figure 2). This *Gm–St* facies association suggests deposition in active channel at the waning flow of a braided channel. The sand from this zone yielded  $26.5 \pm 2.4$  ka OSL age<sup>11</sup>. The *Gm–St* facies zone is overlain by 3–5 m thick rhythmic/cyclic sedimentation of suspended bed load forming alternate 10–30 cm thick massive thinly laminated medium grained sand (*Sm*) and silt/mud (*Fm*) beds (Figure 3a). The primary depositional and erosional sedimentary structures namely cross-laminations/bedding, climbing ripples, irregular channel erosion, lateral spread and slumps are observed in the basal part of the rhythmite (Figure 3). The rhythmite deposits are eroded by sporadic small channel inundations, which deposited poorly sorted coarse sand/granules and mixed sediments with laminations parallel to the channel wall as well as cross-laminations (Figure 3b–d). The influx of channel water also produced small folding and lateral spreading (Figure 3c and d) in cohesive mud beds, whereas the climbing ripples and cross-laminations (Figure 3a and b) are common in coarse sand beds. The rhythmite zone is overlain by massive fine-grained sand and mud (*Fs–Fm*) with upward increase in massive mud content and diminishing internal laminations (Figure 2). The sand in this upper part yielded  $25.2 \pm 1.8$  ka OSL age<sup>11</sup>, suggesting an average sedimentation rate of  $9.2 \pm 4.15$  mm/yr in the section. This high

sedimentation rate is related to the transient phase of summer monsoon intensification during climatic transition from MIS III to MIS II in Himalaya<sup>8</sup> (Figure 1c).

The coarse grained *Gm–St* sediment facies (Figure 2) and presence of climbing ripple and large-scale cross-bedding (Figure 3a and b) in the basal part of the section suggest high-suspended load and carrying capacity in the active channel of the river<sup>12,13</sup>. The confined floodplain of Sub-Himalaya (Figures 1b and 4) is the ideal location for high sediment aggradation during intensified monsoon phase with high fluvial discharge and sediment flux as the channel gradient decreases abruptly. It is observed that in tectonically active terrain, rivers with high fluvial discharge and sediment flux tend to cause rapid incision and erosional avulsion to attain a straighter path<sup>14</sup>. During initial phase of erosional avulsion, when the slope of new and old channels is about the same, both channels are occupied by flow; and with progressing avulsion, the sediment mobilization causes rapid alluviation forming a plug bar at the chute cutoff, which isolates the former channel as abandoned channel<sup>14</sup>. Similar erosional avulsion, growth of plug bars and channel abandonment are observed in the modern Yamuna river (Figure 4a). Uniform incision (Figures 2 and 4a) across climatically varied phases (Figure 1c) is observed in the Dun valley, which suggests that the incision is largely driven by active tectonics of the region<sup>9,10</sup>, and therefore a similar geomorphic setup during the growth of  $T_6$  terrace is expected. The *Gm–St* facies in the lower part of the studied section (Figure 2) represents the active conduit of the channel during  $26.5 \pm 2.4$  ka prior to the channel avulsion. The presence of climbing ripples at the base of the rhythmite deposits (Figure 3a and b) indicates, passing of fluvial regime towards low carrying capacity as a function of either reduced discharge or channel migration to a new course leaving behind the abandoned channel<sup>14</sup>. Accumulation of rhythmic and lacustrine (*Sm* and *Fm* facies) sediments (Figure 2) suggests deposition of suspended sediments in the abandoned channel. The coarser sand (*St*) and erosional structures (Figure 3b–d) towards the lower part of rhythmite zone suggest that the abandoned channel experienced occasional inundation during initial phase of abandonment<sup>13,14</sup>. This scenario would have resulted from a combination of erosional avulsion and plug bar growth due to high sediment load leading to channel isolation. These processes are largely a function of how connected the abandoned channel is to the active river and also depends on seasonal variations in the fluvial discharge as observed during the present day Indian summer monsoon. The overlying mud and silt (*Fm*) were deposited as residual fill in the lacustrine environment of the abandoned channel akin to an ox-bow lake.

Three zones of SSD structures are observed in the rhythmite deposit of the studied section (Figure 2). The SSD structures include loads, slumps, fold and faults including graben, listric fault and a combination of brittle

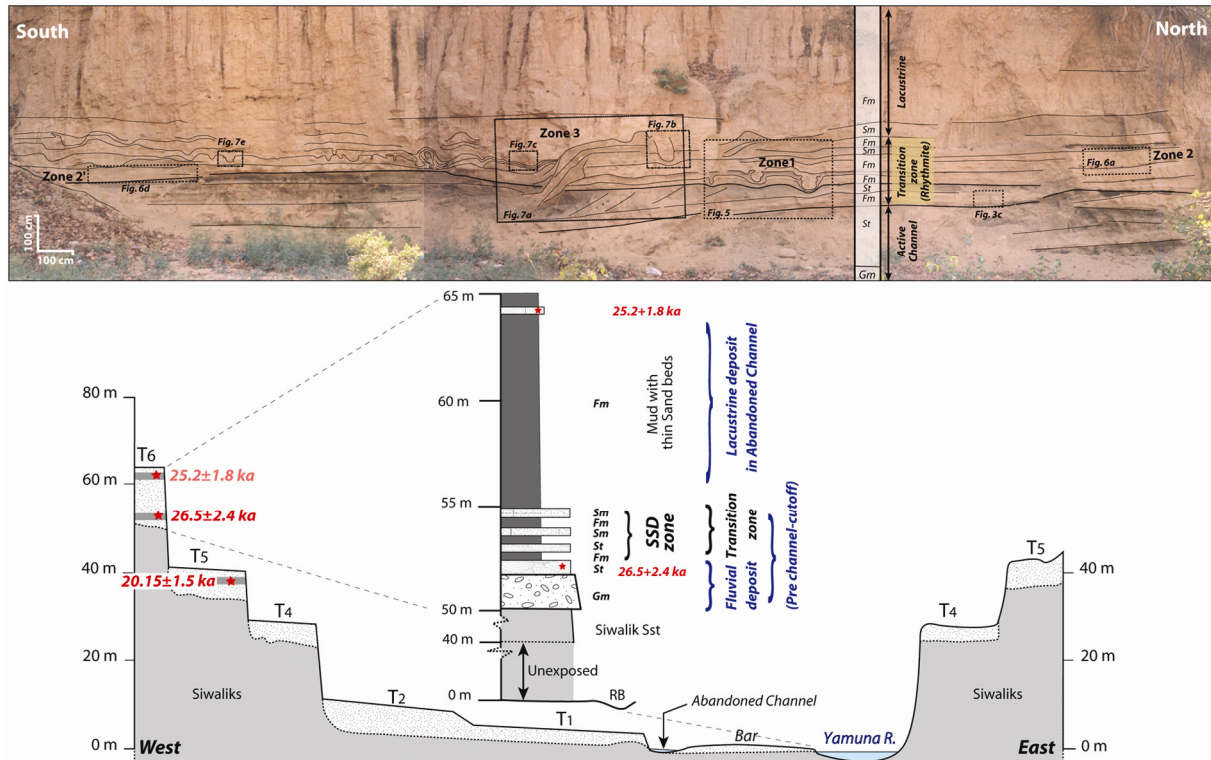


**Figure 2.** The profile section, litho-log and ages of fluvial terraces across Yamuna river along with the outcrop view of the studied section overlaid with litho-facies. Three depositional regimes namely, active channel, fluvial-rhythmite and lacustrine, are distinguished. Note different SSD zones (1 to 3) in the rhythmite and subsequent figure index.

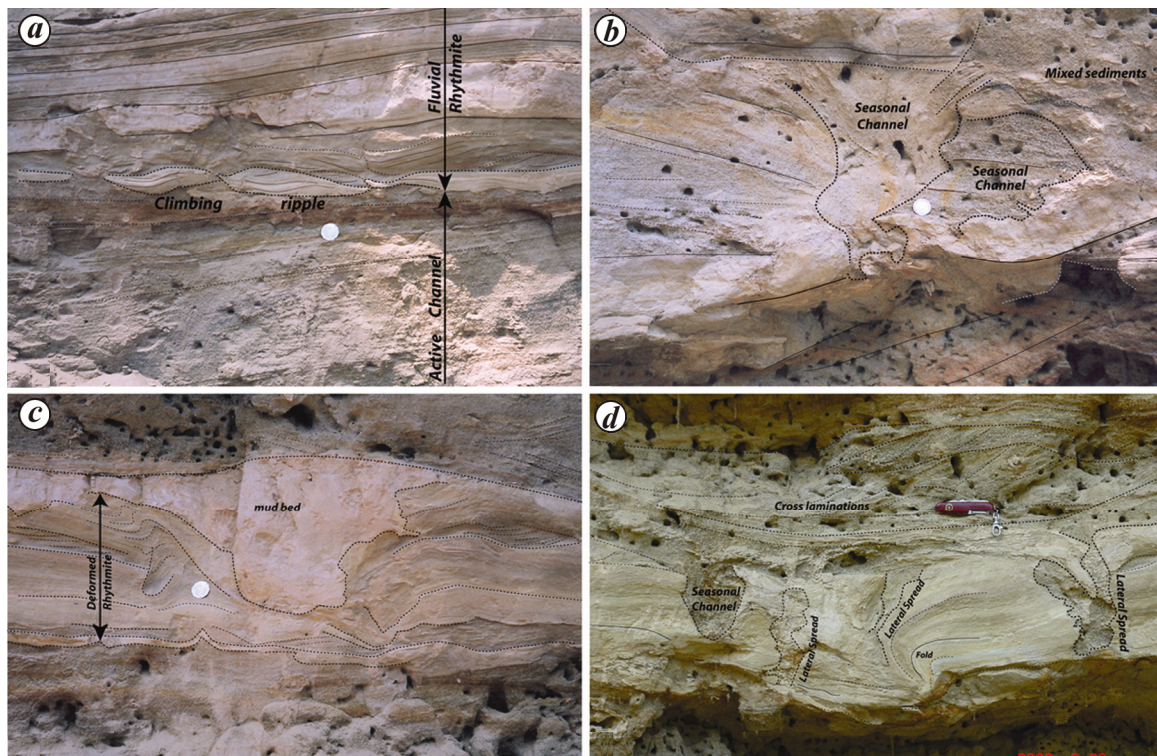


**Figure 3.** Depositional and erosional sedimentary structures observed at the base of the rhythmite zone. *a*, Cross bedding, climbing ripple; *b*, Scour and fill by small channels and sediment mixing; *c*, The scour in deformed rhythmite is occasionally being filled by mud; *d*, Scour and fill, lateral spreading and folding. Note small scale cross-bedding, poorly sorted–unsorted granule and coarse sand suggesting sudden inundation.

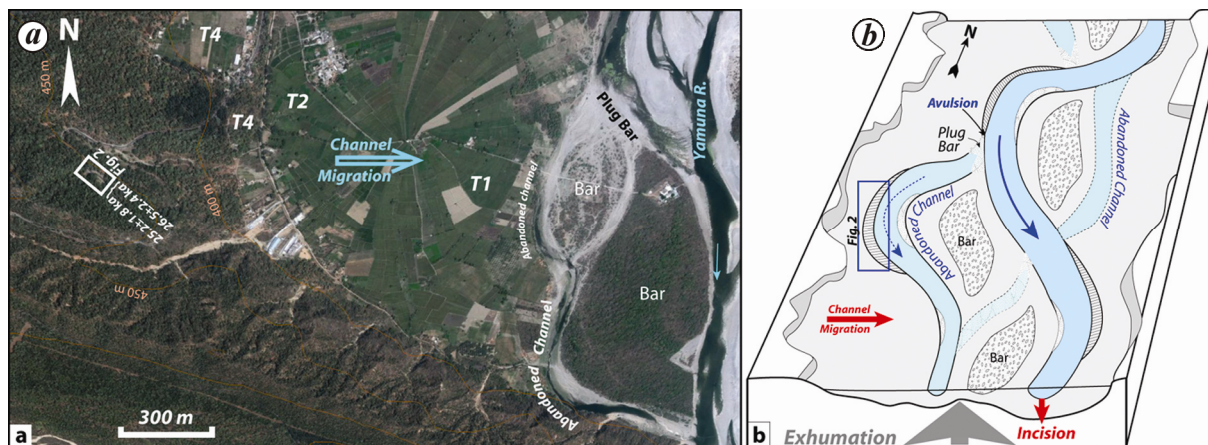


**Figure 4.** *a*, Google image of the studied area showing different terraces suggesting migration and channel incision by river Yamuna. At present the Yamuna river occurs as braided channel with erosional avulsion to attain straighter course and the alluviation causes growth of plug bar leaving behind the abandoned channels that occur like an ox-bow lake. *b*, The schematic section showing growth of ox-bow lake in the abandoned channel in response to the channel migration by erosional avulsion and valley floor incision. The growth of plug bar by sediment flux causes isolation of abandoned channel producing lacustrine depositional setup.

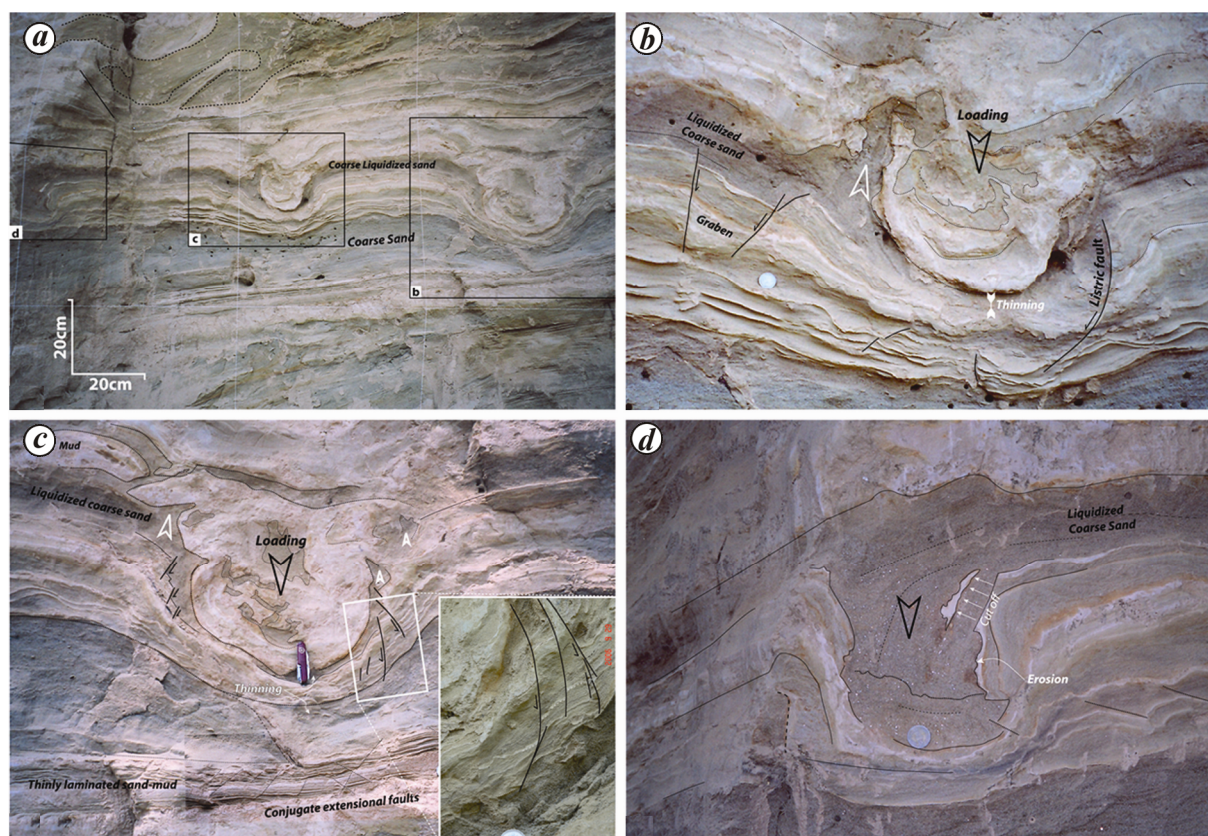


**Figure 5.** *a*, Multiple symmetrical loads in the middle part of the section (SSD zone 1). *b*, The symmetrical load with three dimensional geometry showing down warping of mud bed into the underlying sand, which is pinched away. A series of load structures with upward converging geometry displaced the underlying thinly laminated sand–mud beds (inset). Note the conjugate extensional fault in the thinly laminated sand–mud bed below the load trough. *c*, The load is bordered by listric fault towards one margin and graben at the other suggesting extensional regime towards margin. *d*, The load of coarse sand bed and the liquefied sand corrode the basal mud bed, a part of which is floating in the sand.

faulting and plastic deformation. These SSD zones are invariably bounded by undeformed beds, which mark a period of quiescence after the growth of individual SSD structures.

The SSD zone 1 affects ~50–70 cm thick zone of rhythmic sediments in the middle part of the section (Figure 2) forming a series of load structures with distinct geometry and association (Figure 5*a*). The loads show

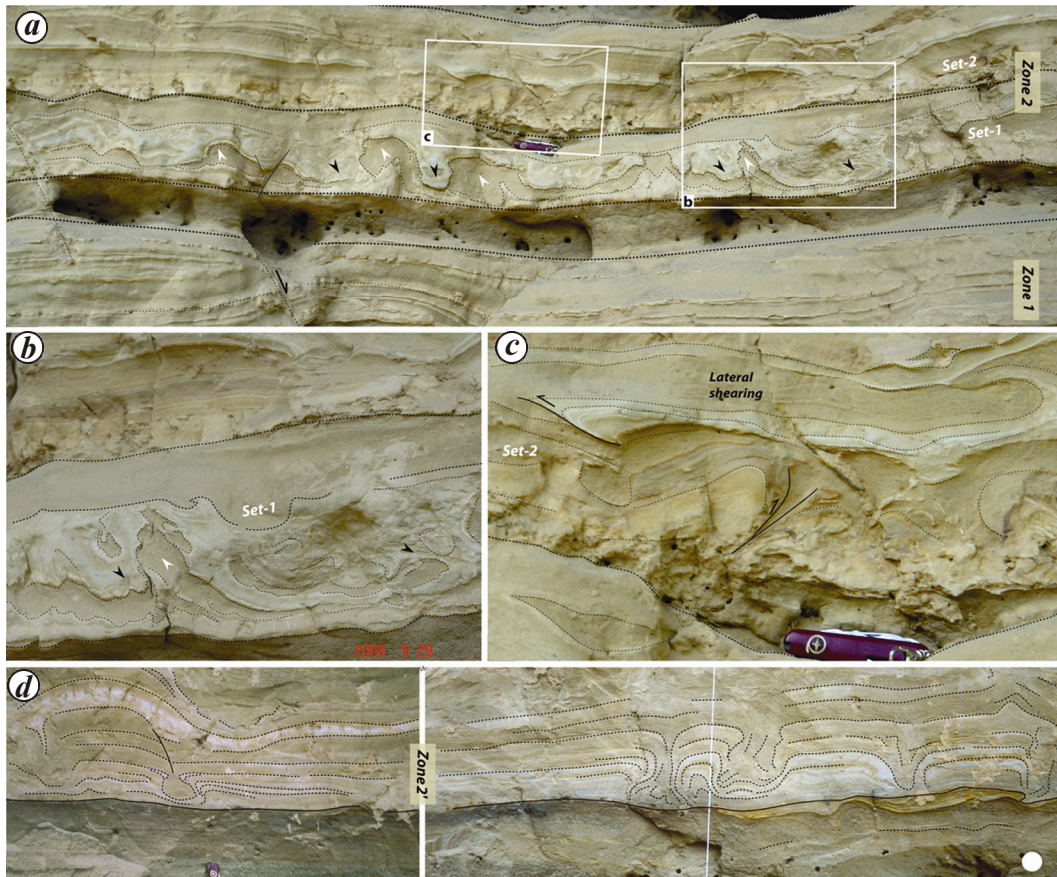


**Figure 6.** SSD zone 2, towards margins of the studied section, constituted of (a) two sets of SSD zones, separated by undeformed sand beds. In the lower set 1 the liquified sand shows upward migration with asymmetric antiformal perturbation (marked by white arrow) and the overlying mud bed shows asymmetric down-warping (marked by black arrow). b, The set 1 containing complex asymmetric synformal down-warping of mud beds is overlain by undeformed sand bed. c, The sand–mud bed showing lateral shearing with small scale reverse faulting and drag fold growth in the set 2. Note the chaotic mixing of the sediments in the middle part. d, The contorted bed, convolution and load like structure towards upstream margin are observed in SSD zone 2'.

symmetrical synclinal down warping of mud–sand beds forming multiple concentric rounded lobes (Figure 5 b and c). The size of the symmetrical ball and pillows varies from ~25 to ~15 cm in vertical dimension (Figure 5) uniformly affecting the mud–sand beds without inter-bed sediment mixing. The basal sand bed pinches away losing internal lamination in the vicinity of the trough of pillows but the lamination remains undisturbed away from the load toe (Figure 5 b and c). Another load in the series involves only the basal sand bed that sinks with partly preserved lamination and the sand cuts through the mud bed (Figure 5 d) suggesting the liquification during deformation. A series of extensional faults with concave-up listric geometry die-out in the bedding plane of the underlying sand–silt beds with decimetre scale displacement (Figure 5 b inset, c) at the basal bulge of the pillow structures is observed in thinly laminated mud–sand beds. Small-scale graben towards margin and a set of conjugate extensional faults beneath the pillow trough are also observed in the thinly laminated sand–silt beds (Figure 5 b). These extensional structures (Figure 5 b and c) are restricted to the

beds underneath and towards the margins of the pillow and are absent elsewhere in the affected bed.

The SSD zone 2 is observed towards the margins of the section, affecting >3 m wide and ~60 cm thick zone (Figure 2) of thinly laminated mud–silt/fine sand beds with complex deformation structures (Figure 6). Towards the northern side of the section, two sets of SSD zones, separated by un-deformed sand beds (Figure 6 a) are observed within SSD zone 2. The lower set shows complex asymmetric folding where the overlying mud beds form a series of synformal lobes and the underlying sand bed occupies the antiformal protuberance (Figure 6 a and b). The sand bed with uneven thickness shows thinning under the synformal trough (Figure 6 b) and the cohesive mud bed shows extensional faulting (Figure 6 a). The sand bed is homogenized losing primary lamination with randomly disseminated mud fragments suggesting liquification of the bed. The overlying SSD set is confined to ~20 cm thick zone of interbedded mud and fine sand beds with drag folding and reverse faulting (Figure 6 a and c). These discreet reverse faults and folds produce

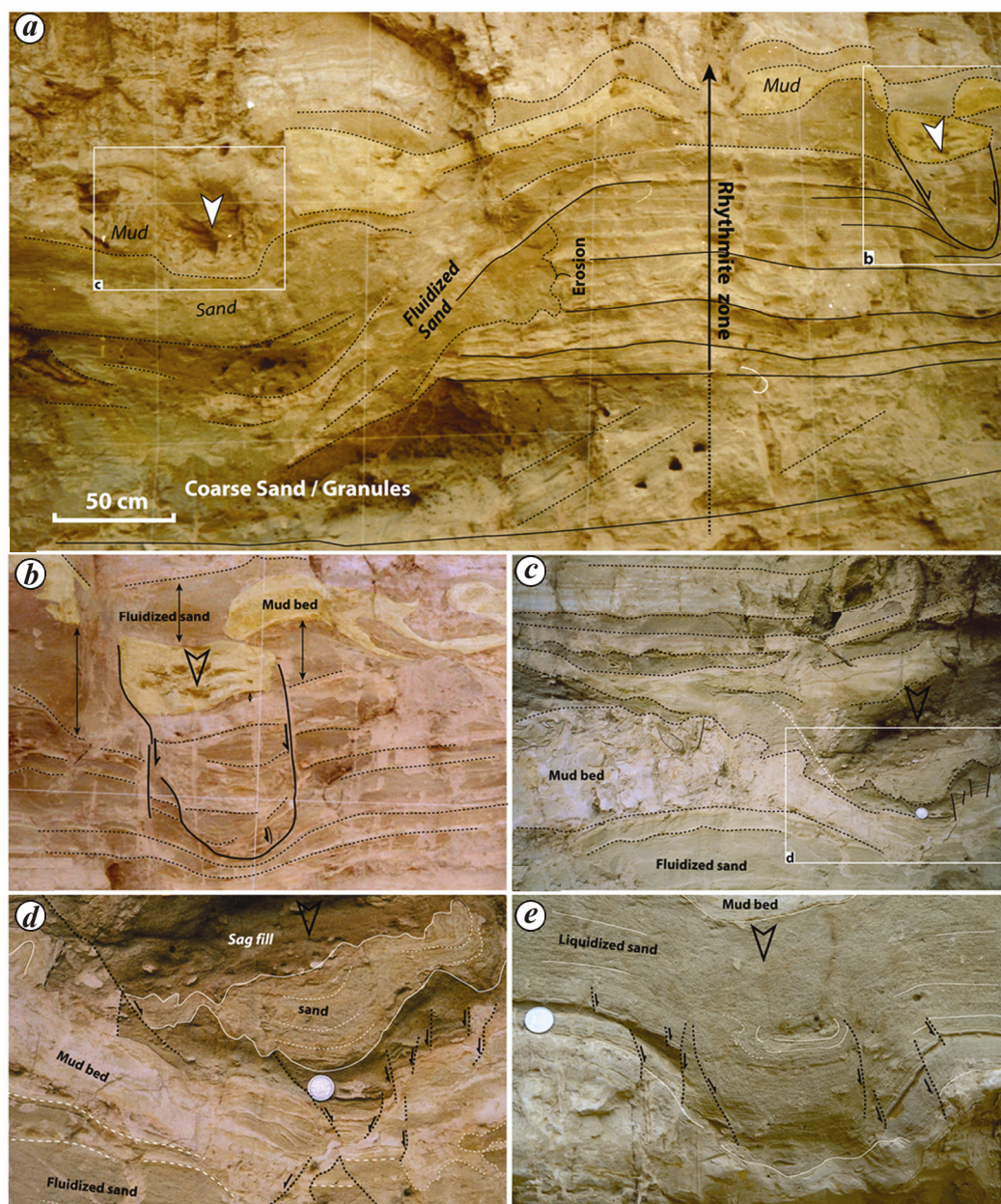


**Figure 7.** The SSD zone 3 with (a) pronounced slump zone affecting the rhythmite deposit in the middle part of the section. The fluidized and homogenized sand in the slump zone corrodes the rhythmite and affects the overlying mud bed, which at places got detached and segregated. b, The uneven thickness of liquidized sand and sagging of detached mud bed led to the pinching of sand in graben zone. c, Complex deformation with the sagging and synformal warping in the hanging wall block of the slump. Note the zone with synformal warping of mud and sand bed is covered by horizontal beds suggesting post deformation deposition. The lamination is preserved in the underlying sand bed, which is liquidized in slump zone. d, The expanded view shows the lower sand–mud beds are faulted with half graben geometry. The overlying sand beds show synformal warping and are unconformably covered by undeformed mixed sediment, which filled the sag. e, The liquidized sand bed shows fault bound synformal sagging with the sub-parallel upward converging faults. The lamination in the upper part of the sand bed is not clear suggesting partial liquidization. These SSD structures are analogous to the gravity driven graben.

complex deformation structures with limited continuity of the beds (Figure 6c). The cohesive nature of mud and sand suggests quasi-plastic deformation and lateral shearing. A series of convolutions is observed in 20–30 cm thick zone of thinly laminated mud–sand beds (Figure 6d) towards the southern margin of the section and are

designated as zone 2' (Figure 2). A series of load-like structures is observed where the coarse-grained sands sank into the fine-grained substratum with synclinal sagging, producing structures similar to the drop structures, contorted bedding, water escape structures with lateral spreading and up-warping (Figure 6d).

The SSD zone 3, at higher stratigraphic level, consists of pronounced slump, chaotic mixing of fluidized sediments and a series of synclinal warp bordered by faults (Figure 7). A zone of homogenized sand devoid of internal laminations descends from the top of the rhythmite zone to the basal coarse sand/granule bed and forms a slump (Figure 7a). The fluidized sand eroded away part of the rhythmite deposits towards the margin and caused sediment mixing (Figure 7a). The fluidized sand bed has also affected the overlying mud bed with complex contortions, pinch and swell and occasionally the detached mud bed sinks into the fluidized sand forming synclinal depressions with faulted margins (Figure 7a and b). These marginal faults are sub-parallel, steeply dipping and show an upward converging pattern. In the hanging wall of the slump, the sand fluidization is less pronounced and lamination is better preserved in sand beds (Figure 7a and c). The mud bed forms synformal depression (Figure 7c) and the basal beds show faulting akin to half graben and the overlying coarse sand bed shows synformal downwarping and marginal faulting (Figure 7d). The depression is filled by fluidized coarse sand mixed with mud specks of horizontal disposition (Figure 7c and d). Further south in the section, the fault-bound synformal depressions are observed in the sand–mud bed (Figure 7e). The steeply dipping faults with centimetre scale displacements have upward converging geometry. The basal mud bed behaves as a discreet brittle layer and the overlying sand as a cohesive bed that occupies a synformal depression with fading lamination towards the core (Figure 7e). These structures are akin to the growth of fault-bound synformal depressions with concurrent plastic deformation in the core (Figure 7b, d and e).

Similar to most of the large Himalayan rivers, the river Yamuna flows as a braided channel in the Sub-Himalaya with significantly reduced stream gradient that produces characteristic landforms and deposits, which act as a repository to the contemporary climate and active tectonic signatures (Figures 1b and 4). The presence of recurrent SSD structures in fluvio-lacustrine sediments suggests that the equilibrium of load to bearing capacity was disturbed by density gradient in sediment column and trigger mechanisms (such as flood surges, rapid sediment loading, dewatering, slope failure, impacts causing shock waves or seismic shear waves), which are some of the realistic possibilities in the present depositional and tectonic setting. The yield strength of the unconsolidated water-saturated sediments is significantly reduced by liquidization that deforms heterolithic clastic sediment by grain flow, cohesive flow and brittle failure<sup>1–7,15</sup>.

In the studied section, all the SSD structures invariably have truncated top and are covered by undeformed sand bed (Figures 5–7), suggesting that the SSD occurred in the uppermost bed at sediment–water interface with a time lag between the successive zones and a recurrent trigger mechanism. The SSD structures in zones 1 and 3

are developed in the middle part of the section where gentle dip of the beds (Figure 2) facilitates pore water migration enhancing the liquidization potential of sediments and thereby making the zone more susceptible to soft sediment deformation (Figure 8a). In general, the load structures tend to develop in reverse density gradient systems<sup>4,5,17</sup>, i.e. sand-on-sand/mud; but the observed load structures involve mud-on-sand (Figures 5 and 6), which is not the reverse density gradient in sediment column. Liquidized sand beds with lateral pinching and homogenization show lateral migration and cohesive mud bed with consistent thickness shows cohesive plastic deformation (Figures 5a, 6a, 7a). Low bearing capacity of liquidized sand facilitates the sinking of cohesive mud bed (Figure 8) to form load structure (Figure 5). Symmetrical loads in SSD zones (Figures 5 and 7) do not show any preferred directional orientation suggesting gravity settlement except in the marginal part (Figure 6a), where the asymmetry is caused by lateral shearing as well. The faulting towards the base and margins of loads invariably involves thinly laminated beds of varying grain size (mud/silt–sand; Figure 4b and c). Beds with varying grain size will cause differential liquefaction, which act as cohesion inhibitors in the beds, leading to the extensional faulting when pore-water pressure exceeds bearing capacity<sup>6,15</sup>. Experiments suggest that a sudden increase in pore water pressure by the application of stress can cause small-scale faulting during late stage deformation<sup>15</sup>. Further, the growth of low angle reverse faults and associated folding (Figure 6a), convolutions and lateral spreads (Figure 6d), towards margins in the SSD zone 2, represent lateral shearing (Figure 8a and b). The most complex deformation is observed in SSD zone 3 (Figure 7a), where the liquidized sand bed with greatly reduced yield strength collapsed in response to a trigger (Figure 8b) and it dissipated the pore water pressure (Figure 8c) through highly porous coarse sand and granule bed in the lower part of the transition zone. The geometry is similar to the half graben and with progressive deformation, the hanging wall develops into a synform folding the overlying cohesive fine grained sediments (Figure 7c and d). The sag is filled with mixed undeformed sediments, which exerts further loading causing extensional faulting at grain size contrast, i.e. the sand–mud interface (Figures 7d, 8d and e). When the system is initially under stress, even the partially liquefied bed may deform<sup>6,15</sup> in response to the coeval stress forming synclinal sag with faulted margins (Figure 7e).

The geomorphic, depositional setup and boundary condition in the sediment column in the studied section possibly suggest interaction of climate-driven fluvio-lacustrine process and active tectonics leading to erosional avulsion, alluviation and channel abandonment (Figure 4b). The abandoned channel remained isolated from the active channel fluvio-dynamics and behaved similar to a ox-bow lake with fluvio-lacustrine depositional setup for

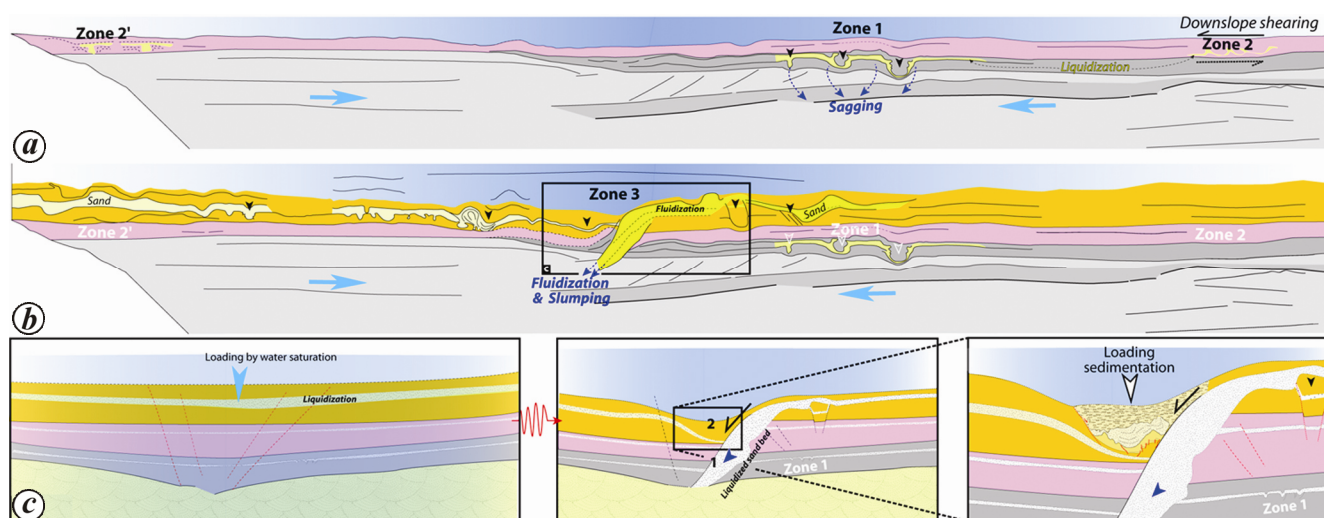


**Figure 8.** Schematic diagram showing sequential growth of different SSD zones in the studied section. *a*, The growth of multiple slumps in zone 1 due to liquidization of sand bed and symmetrical sagging of wet mud bed forming load structure. The growth of low angle reverse fault and folding (zone 2), contortion and lateral spread (zone 2') towards margins is caused by lateral shearing. *b*, The collapse of rhythmite sediment column due to the loss of bearing strength by liquidization and the growth of graben in zone 3. *c*, The process is initiated by liquidization and the localization in the middle part of the section owing to natural slope of the sediment column. *d*, The growth of slump caused deformation akin to the half graben where the hanging wall block sags producing upward converging faults at base at contrasting grain size interfaces and folding of cohesive sediment. The sag is being filled by mixed sediment causing loading and further deformation.

~1000 years during 26–25 ka in Sub-Himalayan range. The Himalayan range experiences great earthquakes every 500–1000 years, moderate–large events at a few decade intervals and numerous micro-seismic<sup>18</sup> events (Figure 1 *a*). The study region experienced large earthquake events during 1991 and 1999 producing soft sediment deformation in contemporary reservoir sediment in a fluvio-lacustrine depositional setting, ~5 km away from the present section<sup>4</sup> as well as the older deposits in the Garhwal region<sup>19</sup>. As the depositional setup, litho-facies association and active tectonics of the region remain the same during the interval of the observation, it is obvious to expect occurrence of a few large earthquake events affecting the rhythmite deposit in the abandoned channel of T<sub>6</sub> terrace. The SSD zones (Figures 5–7) have developed discrete episodes of liquidization and gravity settlement (Figure 8) without observable influence of flood surge, over sedimentation or slope failure in such an active terrain. In view of non-conformity with other trigger mechanisms and ample possibility of episodic loading and liquidization of saturated sediments by discrete and recurrent phases of seismic shear waves, the same is obviously preferred as the trigger mechanism for observed SSD zones in late Quaternary abandoned channel sediments.

The T<sub>6</sub> terrace deposit of the Yamuna river in Sub-Himalaya provides a cliff section where the sedimentation occurred in fluvio-lacustrine environment during  $26.5 \pm 2.4$  to  $25.2 \pm 1.8$  ka at a high sedimentation rate of  $9.2 \pm 4.15$  mm/yr. The sediments show a transition from active channel to lacustrine depositional setting in an

abandoned channel possibly formed by isolation of the cut-off bank by channel avulsion during a phase of intensified summer monsoon. Three discrete zones of SSD structures in the transitional rhythmite in the abandoned channel, suggest that the gravity equilibrium in the sediment column is disturbed by liquidization in the coarse grain lithology by a potential trigger mechanism. As there is no obvious sign of flood surge, rapid sedimentation, overloading or slope failure in the sediment column and in the light of ubiquitous seismicity in the Himalayan belt, seismicity is preferred as potential trigger mechanism. The recurrent earthquake-induced strong ground and shearing would potentially cause differential liquidization in the saturated heterolithic sediment column leading to gravity settlement and growth of SSD structures.

1. Allen, J. R. L., *Sedimentary Structures: Their Character and Physical Basis*, Elsevier, New York, 1982, vol. II, p. 663.
2. Obermeier, S. E., Use for liquefaction induced features for paleoseismic analysis: an overview of how seismic liquefaction features can be distinguished from other features and how their regional distribution and properties of source sediment can be used to infer the location and strength of Holocene paleoearthquakes. *Eng. Geol.*, 1996, **44**, 1–76.
3. Owen, G., Moretti, M. and Alfaro, P., Recognising triggers for soft-sediment deformation: current understanding and future directions. *Sediment. Geol.*, 2011, **235**, 133–140.
4. Pandey, P., Kumar, R., Suresh, N., Sangode, S. J. and Pandey, A. K., Soft-sediment deformation in contemporary reservoir sediment: a repository of recent major earthquake events in Garhwal Himalaya. *J. Geol.*, 2009, **117**, 200–209.
5. Ghosh, S. K., Pandey, A. K., Pandey, P., Ray, Y. and Sinha, S., Soft-sediment deformation structures from the Paleoproterozoic

- Damtha Group of Garhwal Lesser Himalaya, India. *Sediment. Geol.*, 2012, **261–262**, 76–89.
6. Seed, H. B., Soil liquefaction and cyclic mobility evaluation for level ground during earthquakes. *J. Geotech. Eng., Am. Soc. Civil Eng.*, 1979, **105**, 201–255.
  7. Sarkar, S., Choudhuri, A., Banerjee, S., van Loon, A. J. and Bose, P. K., Seismic and non-seismic soft-sediment deformation structures in the Proterozoic Bhandar Limestone, central India. *Geology*, 2014, **20**, 89–103.
  8. Pandey, A. K., Pandey, P., Singh, G. D. and Juyal, N., Climate footprints in the Late Quaternary–Holocene landforms of Dun Valley, NW Himalaya, India. *Curr. Sci.*, 2014, **106**, 245–253.
  9. Thakur, V. C., Pandey, A. K. and Suresh, N., Late Quaternary–Holocene evolution of Dun structure and Himalayan Frontal Fault zone of Garhwal Sub Himalaya, NW India. *J. Asian Earth Sci.*, 2007, **29**, 305–319.
  10. Singh, A. K., Prakash, B., Mohindra, R., Thomas, J. V. and Singhvi, A. K., Quaternary alluvial fan sedimentation in the Dehradun valley piggyback basin, NW Himalaya: tectonic and paleoclimatic implications. *Basin Res.*, 2001, **13**, 449–471.
  11. Dutta, S., Suresh, N. and Kumar, R., Climatically controlled Late Quaternary terrace staircase development in the fold and thrust belt of the Sub Himalaya. *Palaeogeogr., Palaeoclimatol., Palaeoecol.*, 2012, **356–357**, 16–26.
  12. Ashley, G. M., Southardt, J. B. and Boothroyds, J. C., Deposition of climbing-ripple beds: a flume simulation. *Sedimentology*, 1982, **29**, 67–79.
  13. Reineck, H. E. and Singh, I. B., *Depositional Sedimentary Environments*, Springer-Verlag, Berlin, 1973, p. 439.
  14. Slingerland, R. and Smith, N. D., River avulsions and their deposits. *Annu. Rev. Earth Planet. Sci.*, 2004, **32**, 257–285.
  15. Owen, G., Deformation processes in unconsolidated sands. In *Deformation of Sediments and Sedimentary Rocks* (eds Jones, M. E. and Preston, R. M. F.), Geological Society of India Special Publication, 1987, vol. 29, pp. 11–24.
  16. Sims, J. D., Earthquake-induced structures in sediments in Van Norman Lake, San Fernando, California. *Science*, 1973, **182**, 161–163.
  17. Ankettel, J. M., Cegla, J. and Dzulinsky, S., On the deformational structures in systems with reverse density gradients. *Ann. Soc. Geol. Pologne*, 1970, **XL**, 3–30.
  18. Bilham, R., Gaur, V. K. and Molnar, P., Himalayan seismic hazard. *Science*, 2001, **293**, 1442–1444.
  19. Pandey, P. and Pandey, A. K., Active deformation along the Hinna Fault in Uttarkashi region of Garhwal Himalaya. *J. Geol. Soc. India*, 2006, **68**, 657–665.

ACKNOWLEDGEMENTS. We acknowledge financial support from HEART and SHORE programmes of CSIR-NGRI. We appreciate comments from anonymous reviewer, which helped bringing clarity.

Received 23 September 2014; revised accepted 24 February 2015

## Nest site characterization of sympatric hornbills in a tropical dry forest

Ushma Shukla<sup>1</sup>, Soumya Prasad<sup>1,2,5,\*</sup>,  
Mohan Joshi<sup>1,2</sup>, Sachin Sridhara<sup>3</sup> and  
David A. Westcott<sup>4</sup>

<sup>1</sup>Centre for Ecological Sciences, TE-13, Biological Sciences Building, Indian Institute of Science, Bengaluru 560 012, India

<sup>2</sup>Nature Science Initiative, 36, Curzon Road, Dehradun 248 001, India

<sup>3</sup>School of Marine and Tropical Biology, James Cook University, Australia

<sup>4</sup>CSIRO Ecosystem Sciences, Maunds Road, Atherton Qld 4883, Australia

<sup>5</sup>Present address: School of Life Sciences, Jawaharlal Nehru University, New Mehrauli Road, New Delhi 110 067, India

**Hornbills, among the largest and most threatened tropical frugivores, provide important seed dispersal services. Hornbill nest site characteristics are known primarily from wet tropical forests. Nests of the Indian grey hornbill *Ocyrceros birostris* and Oriental pied hornbill *Anthracoceros albirostris* were characterized in a tropical dry forest. Despite *A. albirostris* being twice the size of *O. birostris*, few of the nest cavity attributes were different. *A. albirostris* nests were surrounded by higher proportion of mixed forest and lower sal forest compared to *O. birostris*. In this landscape, the larger *A. albirostris* may prefer to nest in sites with more food plants compared to the smaller *O. birostris*.**

**Keywords:** *Anthracoceros albirostris*, nesting ecology, *Ocyrceros birostris*, tropical forests.

HORNBILLs are a wide-ranging, diverse group of birds occurring in Asia and Africa. Within Asia, 31 species of hornbills are found in a variety of habitats ranging from rainforests to dry and arid zones. Being primarily frugivorous and large-bodied, they consume a wide spectrum of fruit types in varying sizes<sup>1</sup> and are important seed dispersers. They also provide unique dispersal services to several large-seeded plants<sup>1,2</sup>. Despite their ecological importance, our knowledge of hornbill ecology is limited to a few species and to particular landscapes. Most studies examining hornbill ecology emerge from wet tropical forests, although hornbills inhabit a wide range of habitats, including dry tropical forests and human modified landscapes. Since resources required by hornbills, such as fruiting trees and nesting sites may differ significantly across these habitats<sup>3</sup>, it is important to examine their nesting and landscape use in diverse habitats to understand their ecological tolerance and to design appropriate conservation strategies. This knowledge gap is particularly heightened given the special requirements of hornbills for breeding and nesting.

\*For correspondence. (e-mail: prasadsoumya@gmail.com)